Monte Carlo approach to the gas-liquid transition in porous materials

M. Álvarez,* D. Levesque, and J.-J. Weis
Laboratoire de Physique Théorique, Bâtiment 210, Université de Paris–Sud, 91405 Orsay Cedex, France
(Received 1 July 1999)

The gas-liquid transition of a ''quenched-annealed''(QA) system is studied by grand-canonical Monte Carlo simulation. The ''quenched'' particles are hard spheres within configurations chosen randomly from those of an equilibrium hard-sphere system at given density. The fluid particles interact with the matrix particles by a hard-core potential and with each other by a hard-core potential and an additional potential of a Lennard-Jones type. Our results are in good qualitative agreement with various theoretical approaches. With increasing matrix density the critical temperature is lowered compared to that of the bulk system and the gap between the gas and liquid densities narrowed. Our simulations confirm, for this QA system, the possibility of two fluid-fluid transitions substituting for the unique gas-liquid transition of the bulk system. They demonstrate the necessity to average over a significant number of matrix realizations in order to obtain a quantitative location of the phase coexistence lines. [S1063-651X(99)03311-5]

PACS number(s): 05.70.Fh, 64.70.Fx, 02.70.Lq

I. INTRODUCTION

The effect of a disordered porous medium on the phase diagrams of fluids and fluid mixtures has been the subject of intensive experimental and theoretical investigations during the last decade. One major goal of these studies is the understanding of the role played by the diverse underlying mechanisms inducing transitions between fluid phases in such materials. This knowledge should help us to make predictions about the properties of materials of technological interest, in which the random structure of the adsorbent is of crucial importance (catalysis, adsorption separation, filtration and purification, enhanced oil recovery, gel-exclusion chromatography, gel-permeation electrophoresis, etc.). Experiments performed both on high-porosity materials such as silica aerogels [1–8] or low-porosity materials such as Vycor glass [9–16] have shown quite persuasively that the phase behavior of fluids or fluid mixtures in porous material is markedly different from that of their bulk systems under the same conditions, even if the porous medium occupies only a small fraction of the total volume. A striking example is the phase diagram of the ^{3}He-^{4}He mixture: in the bulk mixture the superfluid transition line terminates at a tricritical point at the top of the coexistence curve; inside highly porous (98% porosity) silica gel [6,17] or porous gold [18] the tricritical point is suppressed and the superfluid transition extends to zero temperature. Phase separation into a superfluid ^{4}He-rich phase and a superfluid ^{3}He-rich phase occurs now entirely inside the superfluid region with a regular critical point at the top of the coexistence curve [17].

In single-component fluids such as ^{4}He [2] and N_2 [5] in high-porosity aerogel, a drastic narrowing of the near-critical liquid-vapor curve is observed (of the order of 14 times in ^{4}He, and 3 times in N_2, relative to the bulk system) and the latter is shifted below that of the bulk (no aerogel) system (the shift in critical temperature is 31 mK for ^{4}He [2] and 0.84 K for N_2 [5]). The critical point is displaced towards the phase that is preferentially attracted by the silica strands (liquid phase). A thermodynamic study of phase separation of isobutyric acid and water in silica gel [8] shows that similar behavior is also expected in binary mixtures. Light- and neutron-scattering experiments, performed at constant composition, are less conclusive as far as a true phase separation is concerned, since a metastable state may have been entered when varying temperature towards phase separation. On the other hand, fluid mixture behavior in low-porosity systems, such as Vycor glass, is generally characterized by metastability and slow kinetics. In these systems no macroscopic phase separation is observed, but rather formation of small microdomains rich in either of the two components.

It is clear that the understanding of phase transitions in porous and disordered materials requires simultaneous consideration of confinement, connectivity of the network, randomness, as well as wetting phenomena. Available theoretical approaches have generally privileged only some but not all of these aspects. Thus the random-field Ising model (RFIM) [19] puts the accent on randomness. Although it may explain some of the features observed in high-porosity gels, in particular the decay of the critical density fluctuations, its application to low-porosity Vycor glass has been questioned [20]. The latter system, in which wetting of the pore surfaces is likely to play a major role in preventing macroscopic phase separation, seems more satisfactorily described by the single-pore model [21–23], which completely ignores randomness.

A third theoretical approach devised to get an insight into the equilibrium properties of fluids in porous solids and that, in principle, can include all specific physical effects of disordered media, is based on a model (referred to as a quenched-annealed system) in which fluid particles evolve in a disordered matrix resulting from the quench of an equilibrium configuration of (matrix) particles generated in the absence of the fluid particles [24]. Recent works have shown [25–29] that the thermodynamic and structural properties of such a model can be obtained from a set of integral equations, the so-called replica Ornstein-Zernike (ROZ) equa-

*Permanent address: Instituto de Química Física ''Rocasolano,'' CSIC, Serrano 119, 28006 Madrid, Spain.

tions, an extension of the familiar OZ formalism of equilibrium liquid-state theory [30].

A further advantage of the quenched-annealed (QA) model is that it is well suited for study by computer simulation [31–35]. Several simulation studies dealing with the phase equilibrium of one- and two-component Lennard-Jones (LJ) 12-6 fluids in a matrix modeled by a frozen equilibrium hard-sphere configuration have appeared recently. Those of Page and Monson [33] based on grand-canonical Monte Carlo (GCMC) simulation [36], were meant to be representative of methane in a silica xerogel, and therefore the size of the matrix particles was chosen much larger than that of the fluid particles (size ratio 7.055:1). Evidence is given for two transitions: one is analogous to the bulk liquid-vapor transition, but the coexistence curve is narrower and the critical density and temperature have lower values; the other, occurring at lower temperatures, has less obvious interpretation and is tentatively related to the wetting properties of the fluid in the more confined regions of the matrix [33]. For a purely repulsive matrix-fluid interaction the second transition occurs on the high-density side of the liquid-vapor transition. Snapshots of configurations in the gas and liquid states close to the liquid-vapor coexistence line reveal a fairly inhomogeneous spatial distribution of the fluid particles, the concentration of fluid particles being highest where the matrix density is lowest [33].

The influence of disorder on the structure of the liquid-vapor interface has been investigated by Trokhymchuk and Sokołowski [34] using canonical Monte Carlo (MC) simulations and integral equation theory for the case where fluid and matrix particles have equal size. A reliable coexistence curve, derived from the density profile, could be obtained only at a low density of the matrix. Although the liquid-vapor transition presents similar trends to those observed by Page and Monson, no evidence is found for a second phase transition.

Of considerable interest in view of technological applications is the phase behavior of liquid mixtures in microporous materials. Gordon and Glandt [35] examined the effect of confinement on phase separation of a symmetric immiscible Lennard-Jones (LJ) mixture in a disordered solid matrix. The symmetric nature of the model allowed use of the Gibbs ensemble Monte Carlo technique [36] to locate the liquid-liquid coexistence curve.

In this paper extensive GCMC simulations were carried out on the phase separation of a single-component fluid within a disordered matrix where fluid and matrix particles have hard cores of equal size. For a given temperature, phase equilibrium is obtained for a value of the chemical potential at which the density distribution has bimodal structure with equal peak heights. The coexistence densities will then correspond to the peak positions. Fluid particles interact by means of an additional attractive LJ tail (defined precisely in Sec. II). With this choice of potential, direct comparison can be made with integral equation theory predictions by Kierlik *et al.* [37]. These authors have solved the ROZ equations for various closure relations, including the mean spherical approximation (MSA) and an optimized random phase approximation corrected to obtain the exact second virial coefficient (ORPA$+B_2$). They arrive at the puzzling result that phase diagrams derived from these approximations, though very similar for the bulk system, get qualitatively different as the matrix density increases. In effect, whereas the MSA predicts one phase transition over the range of matrix densities considered, the ORPA$+B_2$ predicts two, one on the high-density side of the phase diagram occurring at a lower temperature. Whereas the extreme phases were identified as vapor and homogeneous liquid phases, the nature of the intermediate phase could not be characterized with certainty. From analysis of the fluid-fluid correlation functions it was mainly concluded that the local packing of the fluid particles in the intermediate and liquid phases is similar [37].

Discrimination between these two approximations was one of the motivations of the present computations. A second aim was to gain insight into the effect on the location of phase coexistence entailed by using a limited set of matrix realizations (generally only one) for the average over disorder, as was the case in most simulation studies reported so far [33–35].

The remainder of the paper is organized as follows. Section II describes the QA model, the interactions between quenched and fluid particles, and gives details on the MC and numerical methods used in the simulations. In Sec. III the results of the simulations are discussed; in particular, the influence of the matrix configuration (size and realization) on the location and nature of the gas-liquid transition is addressed. Finally in Sec. IV the main conclusions and perspectives of the paper are summarized.

II. MOLECULAR MODEL AND SIMULATION DETAILS

The QA model that is considered in this work consists of spherical fluid particles in a disordered matrix obtained from the quench of an equilibrium hard-sphere (HS) configuration. Fluid particles interact with each other by means of a repulsive HS potential and an attractive Lennard-Jones tail truncated at $r_c=2.5\sigma$

$$U_{ff}(r)=\begin{cases}\infty, & r<\sigma\\ -\epsilon, & \sigma\leqslant r<2^{1/6}\sigma\\ 4\epsilon\left[\left(\dfrac{\sigma}{r}\right)^{12}-\left(\dfrac{\sigma}{r}\right)^{6}\right], & 2^{1/6}\sigma\leqslant r\leqslant 2.5\sigma\\ 0, & r>2.5\sigma\end{cases} \tag{1}$$

and with the matrix particles by a purely repulsive interaction

$$U_{fm}=U_{mm}(r)=\begin{cases}\infty, & r<\sigma\\ 0, & r\geqslant\sigma.\end{cases} \tag{2}$$

Matrix and fluid particles have the same size σ. Matrix and fluid-particle configurations were generated independently by standard GCMC sampling [36] in a cubic box of volume V with periodic boundary conditions. Trial MC moves, translation, deletion, or insertion of particles, were performed in a random way with equal probability. For each thermodynamic state characterized by a reduced temperature $T^*=kT/\epsilon$ and chemical potential μ and a given matrix configuration between 2×10^8 and 2×10^9, trial fluid configurations were generated. To locate the liquid-vapor coexistence curve in this given matrix configuration the chemical potential was varied, at fixed temperature, until a bimodal shape of the

number distribution of fluid particles $P(N)$ was obtained. The chemical potential was then refined, using histogram reweighting, to achieve equal heights of the two peaks in $P(N)$. The coexistence densities were then associated with these two peak positions.

Histogram reweighting [38] enables us to obtain the joint distribution for particle number and energy density $p(N,u)$ for any state (μ_1,β_1) from that of a nearby state (μ,β) $(\beta=1/kT)$. From its definition, omitting, for sake of notational simplicity, the dependence on matrix configuration, one has

$$p(N,u)=\frac{e^{\beta\mu N-\beta Vu}\Gamma(N,u)}{\sum_N \int du e^{\beta\mu N-\beta Vu}\Gamma(N,u)}, \tag{3}$$

where $\Gamma(N,u)$ is the density of states and the normalization is equal to the grand-canonical partition function $\Xi(\beta,\mu)$. Approximating $p(N,u)\approx\mathcal{N}^{-1}H(N,u)$, where $H(N,u)$ is the joint histogram for particle number and energy density recorded during the simulation and $\mathcal{N}$ the number of entries, an estimate of $\Gamma(N,u)$ is obtained from

$$\Gamma(N,u)=\frac{\Xi(\beta,\mu)}{e^{\beta\mu N-\beta Vu}}\frac{H_{\beta,\mu}(N,u)}{\mathcal{N}}. \tag{4}$$

As $\Gamma(N,u)$ is independent of β and μ,

$$p_{\beta_1,\mu_1}(N,u)=\frac{e^{\beta_1\mu_1 N-\beta_1 Vu}\Gamma(N,u)}{\Xi(\beta_1,\mu_1)} \tag{5}$$

$$=\frac{\Xi(\beta,\mu)}{\Xi(\beta_1,\mu_1)}e^{(\beta_1\mu_1-\beta\mu)N-(\beta_1-\beta)Vu}\frac{H_{\beta,\mu}(N,u)}{\mathcal{N}} \tag{6}$$

$$=\frac{e^{(\beta_1\mu_1-\beta\mu)N-(\beta_1-\beta)Vu}H_{\beta,\mu}(N,u)}{\sum_N \int du e^{(\beta_1\mu_1-\beta\mu)N-(\beta_1-\beta)Vu}H_{\beta,\mu}(N,u)}. \tag{7}$$

In particular, at fixed temperature, integrating over the energy density,

$$P_{\mu_1}(N)\propto e^{(\beta\mu_1-\beta\mu)N}P_\mu(N). \tag{8}$$

A second technique we made repeatedly use of was multicanonical ensemble sampling [39–41], which can be applied advantageously to enhance crossing of the free energy barrier separating the coexisting gas and liquid phases at subcritical temperatures. Briefly stated, in this method sampling is made from a non-Boltzmann distribution with modified Hamiltonian $\mathcal{H}'=\mathcal{H}+g(N)$ where the function $g(N)$ will be adjusted in such a way that the particle number distribution $P'(N)$ will be nearly flat, implying that, contrary to simple Boltzmann sampling, the interfacial states will be sampled with nearly the same probability as the gas and liquid configurations. The ideal choice fulfilling the preceding requirement would be $g(N)=\ln P(N)$. In practice, $P(N)$ is of course unknown, but an estimate can be made by extrapolation, using the histogram reweighting technique described above, from that of a nearby state [possibly starting from a near critical state where the interfacial tension is low and $P(N)$ therefore obtainable by straightforward Boltzmann sampling]. At the end of the simulation the desired particle number distribution is regained from $P(N)\propto P'(N)e^{-g(N)}$.

III. RESULTS

A. Bulk fluid

For vanishing matrix density $(\rho_m=0)$ the system reduces to a bulk fluid where particles interact through potential (1). The gas-liquid coexistence curve of this system was determined through Gibbs-ensemble Monte Carlo (GEMC) simulations [36,42] in the temperature range $T^*=1.0-1.22$. With this method a total of $N=N_1+N_2$ (in the present circumstances 500) particles are distributed between two boxes of volume V_1 and V_2 with total volume $V=V_1+V_2$ fixed. Chemical (equal chemical potentials in the two boxes) and mechanical (equal pressures) equilibria are then achieved through MC steps involving displacement moves, volume changes, and particle exchanges, keeping the total volume and total number of particles constant. After convergence of the simulation the averages $\langle N_1/V_1\rangle$ and $\langle N_2/V_2\rangle$ will be the coexistence densities. At temperatures $T^*>1.18$ the gas and liquid boxes changed identity and the coexistence densities were determined from the peak positions in the density distribution $P(\rho)$. For each temperature between 120 000 and 500 000 cycles were performed, each cycle consisting of $N=500$ trial translation moves, 250 attempted particle exchanges and one volume change. The densities and chemical potentials of the coexisting phases are summarized in Table I and the coexistence curve shown in Fig. 1 together with the MSA results of Kierlik *et al.* [37].

The GEMC method does not allow a precise estimate of the critical temperature [43,44]. A customary procedure for obtaining an estimate of the critical parameters T_c and ρ_c is to fit the coexistence data to the scaling law

$$\rho_l-\rho_g=B(T-T_c)^\beta \tag{9}$$

and the law of rectilinear diameters

$$(\rho_l+\rho_g)/2=\rho_c+A(T-T_c), \tag{10}$$

where, in the present case, β is the critical exponent of the 3D Ising universality class ($\beta\approx0.3258$ [45]). Care should, though, be in order when applying this procedure. Gibbs ensemble simulations are generally performed for rather small system sizes, therefore suppressing long-range density fluctuations. As a result crossover from nonclassical to mean-field (classical) behavior is expected at some unknown crossover temperature. For this reason data close to the (apparent) critical temperature are generally discarded in the fit.

The critical temperature and density are close to $T^*=1.225$ and $\rho^*=0.315$. Due to the wider range of the attraction near the core region this critical temperature is somewhat higher than that of the Lennard-Jones system truncated at 2.5σ [40].

TABLE I. Liquid-vapor equilibrium of the bulk fluid ($\rho_m^*=0$) from GEMC simulation. Results obtained from the reference hypernetted chain equation [30] have been included.

T^*	Cycles	ρ_g^*	$\beta\mu_g$	ρ_l^*	$\beta\mu_l$	$\beta\mu_{RHNC}$
1.22	220 000	0.20(2)	−2.85(4)	0.42(2)	−2.86(4)	
1.21	384 000	0.180(14)	−2.87(4)	0.45(2)	−2.87(4)	
1.20	574 000	0.165(10)	−2.85(5)	0.491(15)	−2.86(5)	
1.19	370 000	0.145(7)	−2.89(4)	0.502(10)	−2.89(4)	
1.175	171 000	0.129(5)	−2.95(4)	0.524(8)	−2.95(4)	
1.15	129 000	0.102(5)	−3.06(3)	0.554(10)	−3.05(3)	−3.000
1.10	550 000	0.081(6)	−3.19(3)	0.620(10)	−3.19(3)	−3.195
1.05	120 000	0.059(6)	−3.40(3)	0.671(13)	−3.40(3)	−3.414
1.00	230 000	0.038(8)	−3.67(3)	0.697(10)	−3.67(3)	−3.664

B. Volume 500

A first set of GCMC simulations was performed at volume $500\sigma^3$ for four values of the porosity corresponding to matrix densities $\rho_m^*=\rho_m\sigma^3=0.026$, 0.046, 0.15, and 0.30. As in previous work only one matrix configuration was considered. For fixed matrix configuration and a temperature estimated to be close to the critical temperature, the chemical potential was varied until a bimodal structure of the particle number distribution $P(N)$ was found. The combined histogram for particle number and energy density was recorded and the histogram reweighting technique described in Sec. II applied to adjust the chemical potential to obtain equal peak heights in $P(N)$. The coexistence densities were then associated with the positions of these two peaks. The coexistence densities and chemical potentials are summarized in Table II and the coexistence curves for different matrix densities and the bulk fluid compared in Fig. 1 with theoretical results [37]. With increasing matrix density, the critical temperature decreases, as expected in a confined system [46], and the coexistence curve narrows. The critical density shifts towards the gas side. These qualitative trends are in agreement with previous simulations [33] and experimental observations, although the narrowing of the coexistence curve is less pronounced as, for instance, in He and Ne [2,5]. Moreover, the results are in semiquantitative agreement with theoretical predictions based on the MSA approximation [37].

However, despite the qualitative agreement with theoretical calculations, experience, and simulations of similar systems, a quantitative assessment of this location of the gas-liquid transition can only be assured if the influence of the matrix configurations on this location is determined and, moreover, finite-size effects are evaluated. To examine the

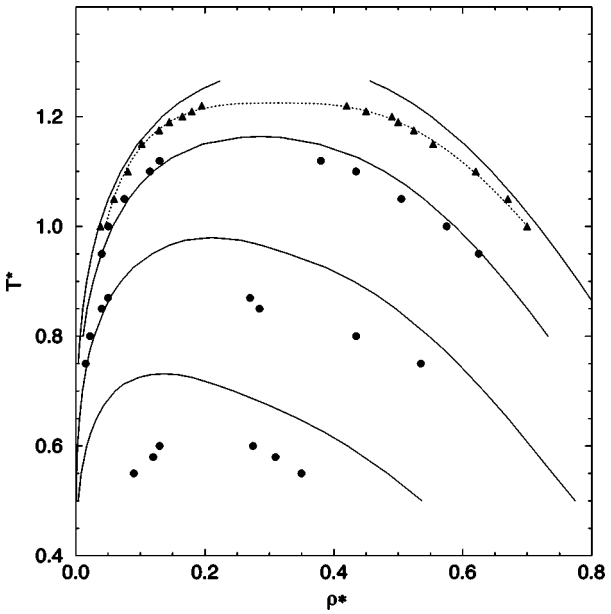

FIG. 1. Coexistence curves for matrix densities $\rho_m^*=0$ (bulk fluid; triangles), 0.046, 0.15, and 0.30 (from top to bottom; solid circles). Results at finite matrix density are for volume $V=500\sigma^3$ and correspond to one matrix configuration (albeit different for each temperature value). It should be noted that the coexisting states on the low-density side of the coexistence curve at $\rho_m^*=0.30$ correspond to the inhomogeneous density phase (see text). The solid lines are the MSA results of Kierlik *et al.* [37] for $\rho_m^*=0$, 0.05, 0.15, and 0.30, respectively (from top to bottom). The dotted line is the fit of the bulk coexistence curve to Eqs. (9) and (10).

TABLE II. Coexistence densities and chemical potential at volume $V/\sigma^3=500$. All results are obtained with one matrix configuration. ρ_g^*, ρ_i^*, and ρ_l^* denote the densities of the gas, inhomogeneous fluid, and liquid phases, respectively. For each state the number of trial configurations was 8×10^8.

ρ_m^*	T^*	ρ_g^*	ρ_i^*	ρ_l^*	$\beta\mu$
0.026	1.00	0.04		0.635	−3.4262
0.026	1.05	0.06		0.595	−3.1956
0.026	1.10	0.09		0.530	−2.9911
0.026	1.15	0.15		0.450	−2.8150
0.026	1.18	0.17		0.380	−2.7315
0.046	0.95	0.04		0.625	−3.5045
0.046	1.00	0.05		0.575	−3.2525
0.046	1.05	0.075		0.505	−3.0343
0.046	1.10	0.115		0.435	−2.8470
0.046	1.12	0.13		0.38	−2.7843
0.15	0.75	0.015		0.535	−3.7123
0.15	0.80	0.022		0.435	−3.3487
0.15	0.85	0.040		0.285	−3.0684
0.15	0.87	0.050		0.26	−2.9767
0.30	0.50	0.085		0.39	−4.0440
0.30	0.55		0.09	0.35	−3.3890
0.30	0.58		0.12	0.31	−3.0318
0.30	0.60		0.13	0.275	−2.8252

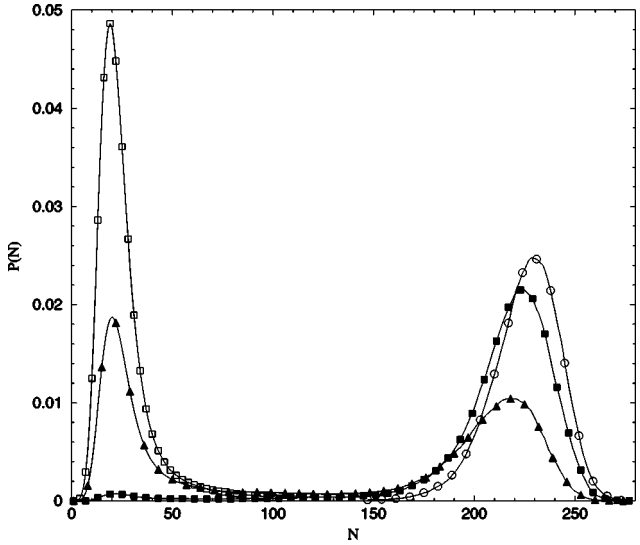

FIG. 2. Fluid particle distribution in matrix configuration B (cf. Table III) for $\beta\mu=-3.0365$ (open squares), $\beta\mu=-3.0159$ (solid triangles), $\beta\mu=-2.9957$ (solid squares), and $\beta\mu=-2.9759$ (open circles).

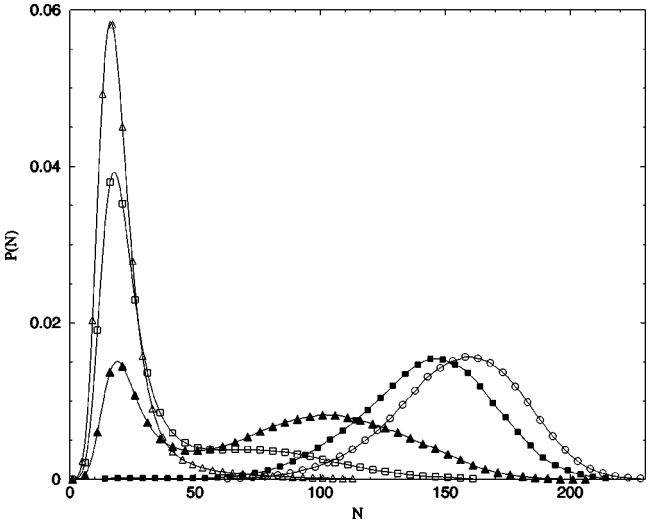

FIG. 4. Fluid particle distribution in matrix configuration C (cf. Table III) for $\beta\mu=-3.1011$ (open triangles), $\beta\mu=-3.0640$ (open squares), $\beta\mu=-3.0365$ (solid triangles), $\beta\mu=-2.9957$ (solid squares), and $\beta\mu=-2.9759$ (open circles).

influence of the matrix configuration on the location of the gas-liquid transition, we determined the chemical potentials corresponding to the equilibrium of the two phases as well as the corresponding densities for different matrix configurations of density $\rho_m^*=0.15$ and temperature $T^*=0.85$. Figures 2–4 show the evolution of the histograms $P(N)$ as a function of the chemical potential $\beta\mu$ for three of these configurations. They show quite convincingly that the values of $\beta\mu$ and the densities of the phases in equilibrium, in particular the dense phase, differ notably with configuration. Equilibrium is found at $\beta\mu\approx-3.015$, -3.058, and -3.0366 for a gas density close to 0.04 and high-density phases of densities 0.46, 0.15, and 0.24, respectively. When $\beta\mu$ increases from its coexistence values the histograms $P(N)$ vary in quite different ways. In particular, Fig. 3 gives evidence of the existence of large density fluctuations, a behavior not present in the two other configurations, which seems indicative of a fluid-fluid transition in this density range. Table III summarizes the properties of phase equilibrium, identified, as described above, by the values of $\beta\mu$ at which $P(N)$ has two maxima of equal height, for the eight configurations studied at matrix density $\rho_m^*=0.15$, and temperature $T^*=0.85$.

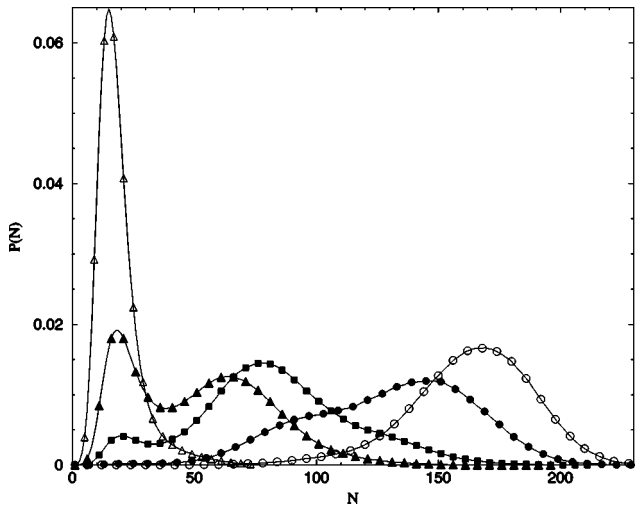

FIG. 3. Fluid particle distribution in matrix configuration H (cf. Table III) for $\beta\mu=-3.1582$ (open triangles), $\beta\mu=-3.0683$ (solid triangles), $\beta\mu=-3.0365$ (solid squares), $\beta\mu=-2.9957$ (solid circles), and $\beta\mu=-2.9565$ (open circles).

The different coexistences seem qualitatively different. As a matter of fact, the phase of density $\rho_l^*\sim0.15-0.20$ in equilibrium with a gas of density $\rho_g^*\sim0.04$ corresponds, as shown by a snapshot of a configuration in Fig. 5, to a very inhomogeneous filling of the matrix. In this phase most of the fluid particles are localized in a specific subvolume, which, for given T^* and $\beta\mu$, occupies the same position in the matrix configuration during the MC run. On the contrary, the fluid phase of density $\rho_l^*\sim0.4-0.5$, also in equilibrium with a gas of density $\rho_g^*\sim0.04$, corresponds to a homogeneous occupation of the volume accessible to the fluid particles (cf. Fig. 6). These findings are compatible with the existence of two phase transitions similar to those discussed

TABLE III. Coexistence densities and chemical potentials at temperature $T^*=0.85$ for eight different matrix configurations $(A,\ldots,H)$ at density $\rho_m^*=0.15$. The volume is $V/\sigma^3=500$. ρ_g^*, ρ_i^*, and ρ_l^* denote the densities of the gas, inhomogeneous fluid, and liquid phases, respectively.

Configuration	ρ_g^*	ρ_i^*	ρ_l^*	$\beta\mu$
A	0.04		0.46	-2.9479
B	0.04		0.44	-3.0129
C	0.04	0.21		-3.0297
D	0.04		0.41	-2.9477
E	0.04	0.36		-3.0597
F	0.04		0.47	-2.9876
G	0.04	0.29		-3.0684
H	0.04	0.14		-3.0591

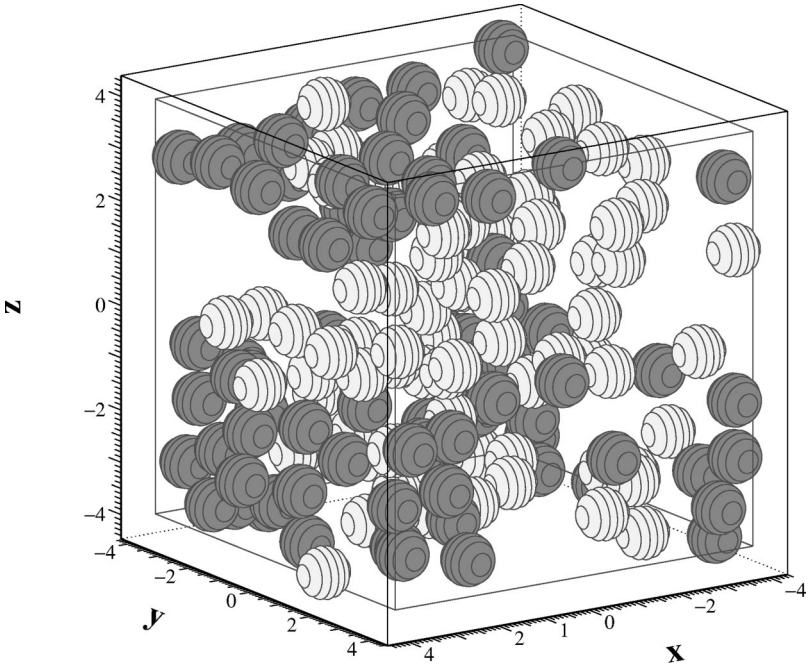

FIG. 5. Snapshot of a configuration corresponding to matrix H (cf. Table III) and fluid density $\rho_i^*=0.14$. The light and dark spheres represent the matrix and fluid particles, respectively. The box lengths are in units of σ.

by Page and Monson [33], one between a gas and an inhomogeneous fluid phase, the second between this latter phase and a homogeneous fluid, as attested, in particular, by the histograms shown in Fig. 3 for $\beta\mu > -3.058$. The possibility of this second phase equilibrium is confirmed by the results for $\rho_m^*=0.30$. For the matrix configurations considered at this density (one for each temperature) the values of ρ_g^* seem notably higher than for $\rho_m^*=0.15$ (cf. Fig. 1). Examination of the snapshot in Fig. 7 of the arrangement of fluid particles in this low-density phase at $T^*=0.55$ shows that these particles are localized in a subvolume of the matrix forming a microdrop of liquid.

In summary, the simulations performed at volume $V/\sigma^3=500$ show unambiguously that phase coexistence is greatly affected by the configuration of the solid matrix and give evidence for the possibility of equilibrium between three types of phases.

C. Volume 1000

To assess the reliability of these results we investigated a system with matrix density $\rho_m^*=0.15$ and temperature $T^*=0.8$ with a larger volume $V=1000\sigma^3$. For this state the $V=500\sigma^3$ system showed a clear liquid-gas transition. Six different matrix configurations, marked $a-f$ in Table IV, were considered. In each case phase equilibrium was achieved by varying the chemical potential until equal peak heights in $P(N)$ were obtained. In accord with the results for

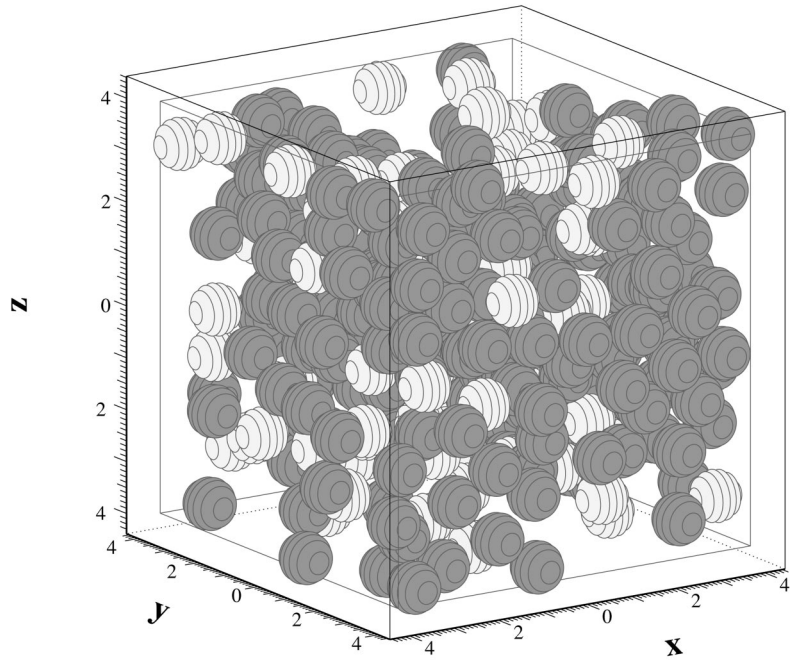

FIG. 6. Snapshot of a configuration corresponding to matrix B (cf. Table III) and fluid density $\rho_l^*=0.44$. The light and dark spheres represent the matrix and fluid particles, respectively. The box lengths are in units of σ.

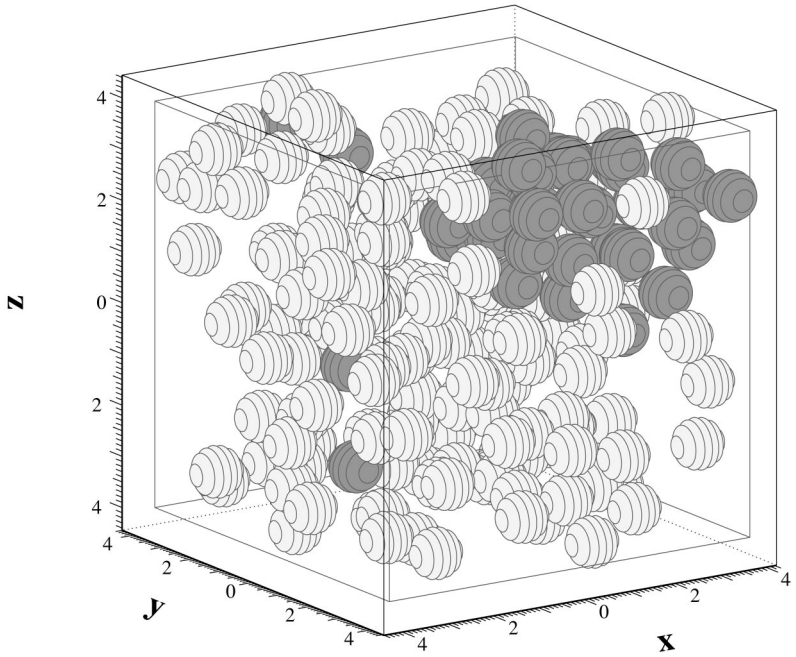

FIG. 7. Snapshot of a configuration for matrix density $\rho_m^*=0.30$, temperature $T^*=0.55$, and fluid density $\rho_i^*=0.09$ (cf. Table II). The light and dark spheres represent the matrix and fluid particles, respectively. The box lengths are in units of σ.

the smaller volume three different situations were encountered (cf. Table IV):

(i) In three cases (a,b,c) a transition between a low-density gas ($\rho_g^*\approx 0.03$) and a homogeneous liquid ($\rho_l^*\approx 0.5$) is observed.

(ii) In two cases (d,e) equilibrium is found to occur between a gas at density 0.03 and a ''liquid'' at a density considerably lower ($\rho^*=0.13$ for matrix configuration d, $\rho^*=0.30$ for matrix configuration e) than for the preceding cases. Snapshots of configurations of the system reveal that the fluid particles are not distributed in a homogeneous way in the matrix, but extensive regions in the matrix have very low fluid density. By increasing the chemical potential for these matrix realizations the position of the peak in $P(N)$ corresponding to this ''droplet'' arrangement shifts to higher density and the size of the droplet increases until eventually a homogeneous distribution of the fluid particles is obtained.

(iii) For the matrix labeled f, at chemical potential $\beta\mu=-3.298$, $P(N)$ shows a three-peak structure with peak positions corresponding to $\rho^*=0.03$, 0.16, and 0.48, respectively, the fluid densities already observed in the previous cases (cf. Fig. 8). For the chosen value of $\beta\mu$ the peak heights are different, but by varying the chemical potential equality of either, the two low-density peaks or the two high-density peaks can be achieved.

TABLE IV. Coexistence densities and chemical potentials for six different matrix configurations (a,b,...,f) at density $\rho_m^*=0.15$ and temperature $T^*=0.80$. The volume is $V/\sigma^3=1000$. $\mathcal{N}_c$ is the number of trial configurations. ρ_g^*, ρ_i^*, and ρ_l^* denote the densities of the gas, inhomogeneous fluid, and liquid phases, respectively.

Configuration	$\mathcal{N}_c$	ρ_g^*	ρ_i^*	ρ_l^*	$\beta\mu$
a	10^9	0.03		0.50	-3.265
b	2×10^9	0.03		0.51	-3.182
c	16×10^8	0.03		0.50	-3.2702
d	10^9	0.025	0.13		-3.352
e	8×10^8	0.03	0.30		-3.393
f	2×10^9	0.03	0.16	0.48	-3.298

D. Volume 4000

A still larger system of volume $V=4000\sigma^3$ has been studied by piecing together the eight different matrix configurations considered for volume 500. Overlaps between particles of the different matrix configurations occurring at the common interfaces after assembling, taking into account the periodic boundary conditions, were eliminated by a maximum displacement of 0.42σ of the overlapping spheres. In considering such a matrix configuration our aim was to show that, if for given chemical potential and temperature one of the subvolumes of the matrix is typically occupied by gas (or liquid), this property would persist when the subvolume is

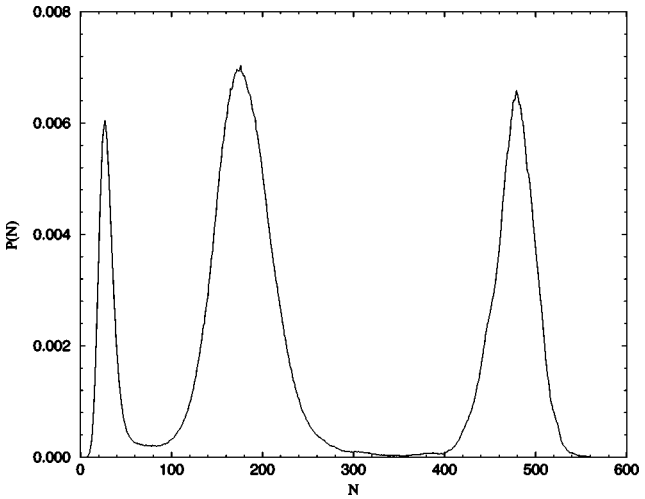

FIG. 8. Fluid particle distribution in matrix configuration f (cf. Table IV) ($\rho_m^*=0.15$, $T^*=0.80$, $V/\sigma^3=1000$). The chemical potential is $\beta\mu=-3.298$.

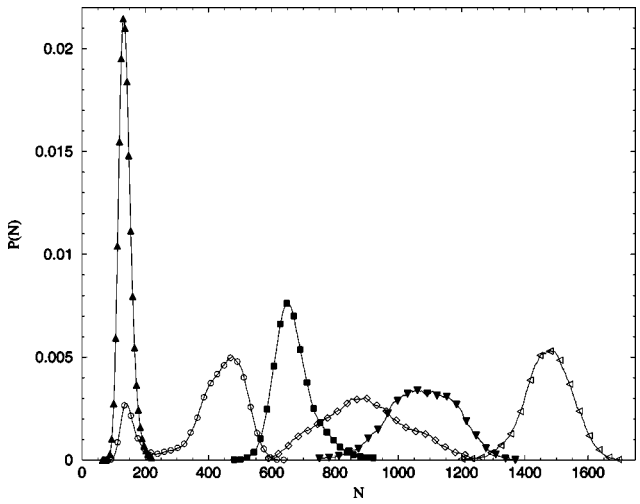

FIG. 9. Variation of the fluid particle distribution for $\rho_m^*=0.15$, $T^*=0.85$ and volume $V/\sigma^3=4000$ with the values of the chemical potential: $\beta\mu=-3.182$ (solid triangles up), $\beta\mu=-3.158$ (open circles), $\beta\mu=-3.068$ (solid squares), $\beta\mu=-3.047$ (diamonds), $\beta\mu=-3.037$ (solid triangles down), and $\beta\mu=-2.995$ (open triangles left).

included in a matrix configuration of larger size. Such an eventuality would obviously speak in favor of the existence of a stable fluid phase associated with a large inhomogeneity of the local density.

At $T^*=0.85$ and $\rho_m^*=0.15$ (i.e., the density of each of the eight subconfigurations) we have calculated the histograms $P(N)$ for $\beta\mu$ varying from -3.182 to -2.976. The histograms obtained for $\beta\mu=-3.182$, -3.158, -3.068, -3.047, -3.037, and -2.996 are shown in Fig. 9. They show the evolution of the filling of the matrix by the fluid from a gas phase at density 0.04 to a liquid phase of density 0.35–0.40. Between these two densities one observes, for $\beta\mu=-3.158$, a histogram characteristic of an equilibrium between a gas of density $\rho_g^*\approx 0.04$ and a phase with density ≈ 0.14, then, for $\beta\mu$ varying between -3.124 and -3.058, a histogram with a single peak of narrow width. For $\beta\mu$ approximately in the range -3.047 to -3.037 the histograms correspond to states presenting large density fluctuations and, for $\beta\mu\approx -2.996$ and larger values, histograms with a single narrow peak are found again. The differences in occupation by the fluid particles of each subvolume can be determined by calculating the histograms associated with the corresponding subconfigurations at the same values of the chemical potential mentioned above. The histograms $P(N)$ for the eight subvolumes at $\beta\mu=-3.158$, -3.068, and -3.037 are shown in Figs. 10–12, respectively. From these three cases it is clearly seen that the different subvolumes are occupied in a very different way by the fluid particles. The evolution of the occupation of the different subvolumes with $\beta\mu$ demonstrates, in agreement with the results at volume $V/\sigma^3=500$, that for each of these subvolumes the dense phase appears at different values of $\beta\mu$. Moreover, in spite of the interactions between the fluid particles located in the different subvolumes, the order in which the dense phases appear in the isolated matrix subconfigurations is conserved in the larger volume (cf. Table III).

The evolution of $P(N)$ of both the total volume and the subvolumes proves again the existence of two coexistences, first between a gas phase and an inhomogeneous fluid phase followed by that between the latter phase and a homogeneous fluid phase of higher density. The existence of a range

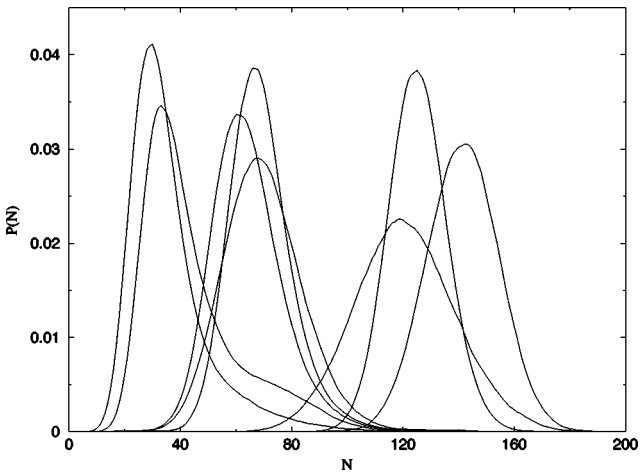

FIG. 11. Fluid particle distributions in the eight subvolumes of the $V/\sigma^3=4000$ system at chemical potential $\beta\mu=-3.068$.

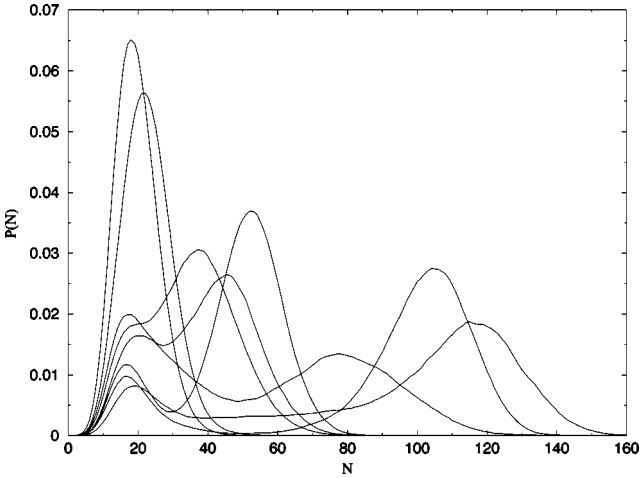

FIG. 10. Fluid particle distributions in the eight subvolumes of the $V/\sigma^3=4000$ system at chemical potential $\beta\mu=-3.158$.

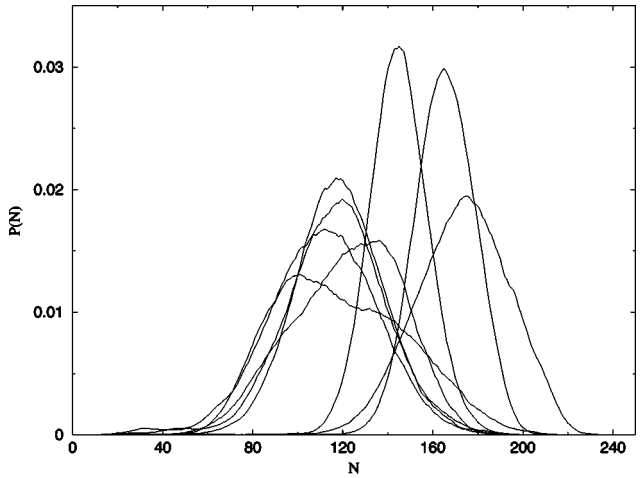

FIG. 12. Fluid particle distributions in the eight subvolumes of the $V/\sigma^3=4000$ system at chemical potential $\beta\mu=-3.036$.

of $\beta\mu$ values for which the inhomogeneous fluid phase is stable is also confirmed by the occurrence of $P(N)$ histograms (typical of a stable phase) having a single peak of small width for $\beta\mu$ between -3.124 and -3.079.

In conclusion the computations made at the volume $V=4000\sigma^3$ enabled us to verify that the qualitative behavior of the fluid, as expected from the previous simulations at smaller volumes, remained stable with respect to an increase of the total volume by a factor of 8.

IV. CONCLUSION

Our simulations have shown that grand-canonical sampling combined with a histogram reweighting technique allows the location of equilibrium between fluid phases in the presence of disorder. Thus for the fluid investigated in this work two types of coexistence between fluid phases have been unambiguously identified when determined with a single realization of the disorder. It seems remarkable that, although the matrix of quenched particles used in our study differs in particle size and interaction between the matrix and fluid particles from that considered by Page and Monson [33], the observation of these three phases are in qualitative agreement with the results of these authors.

The present findings seem also to be corroborated by theoretical calculations based upon the ORPA$+B_2$ approximation [37]. For the matrix density $\rho_m^*=0.15$ and temperature $T^*=0.80$ the intermediate phase occurs in a narrow density and temperature range. It should be noted, however, that the theoretical results are very sensitive to the approximation used. Neither MSA nor the higher-order approximation ORPA$+B_2+B_3$ predict this intermediate phase at $T^*=0.80$ [37].

It would seem that our simulations, especially those obtained for the volume $V/\sigma^3=4000$, allow for an interpretation of the existence of the inhomogeneous fluid phase. It is due to the diversity of the values of the chemical potential at which the fluid goes from the gas to the liquid phase in subvolumes of typical size equal to a few tens of molecular diameters. This variety of transition chemical potentials at this microscopic scale is susceptible to occurrence in numerous types of solid matrices and makes plausible the existence of inhomogeneous fluid phases, such as those identified by Page and Monson [33] and in the present work, in a large class of porous material.

The important differences entailed by the matrix in the values of the densities of the coexisting phases, for example, enforce the conclusion that an average over a significant number of matrix configurations is necessary to obtain a quantitative location of the coexistence curves and to define the domains of the stability or metastability of the different phases. Performing such an average represents a considerable numerical task, which we plan to tackle in future work.

ACKNOWLEDGMENTS

We thank M.-L. Rosinberg for discussion and E. Kierlik for providing the MSA results of Fig. 1. M.A. acknowledges financial support from the Center National de la Recherche Scientifique (CNRS) for her stay at the Laboratoire de Physique Théorique. She also wants to thank the laboratory for its kind hospitality. Computing time on the CRAY C-98 was granted by the Institut de Développement et de Ressources en Informatique (IDRIS). The Laboratoire de Physique Théorique is Unité Mixte de Recherche No. 8627 of CNRS.

[1] J. V. Maher, W. I. Goldburg, D. W. Pohl, and M. Lanz, Phys. Rev. Lett. **53**, 60 (1984).
[2] A. P. Y. Wong and M. H. W. Chan, Phys. Rev. Lett. **65**, 2567 (1990).
[3] B. J. Frisken, F. Ferri, and D. S. Cannell, Phys. Rev. Lett. **66**, 2754 (1991).
[4] B. J. Frisken and D. S. Cannell, Phys. Rev. Lett. **69**, 632 (1992).
[5] A. P. Y. Wong, S. B. Kim, W. I. Goldburg, and M. H. W. Chan, Phys. Rev. Lett. **70**, 954 (1993).
[6] S. B. Kim, J. Ma, and M. H. W. Chan, Phys. Rev. Lett. **71**, 2268 (1993).
[7] B. J. Frisken, F. Ferri, and D. S. Cannell, Phys. Rev. E **51**, 5922 (1995).
[8] Z. Zhuang, A. G. Casielles, and D. S. Cannell, Phys. Rev. Lett. **77**, 2969 (1996).
[9] M. C. Goh, W. I. Goldburg, and C. M. Knobler, Phys. Rev. Lett. **58**, 1108 (1987).
[10] S. B. Dierker and P. Wiltzius, Phys. Rev. Lett. **58**, 1865 (1987).
[11] P. Wiltzius, S. B. Dierker, and B. S. Dennis, Phys. Rev. Lett. **62**, 804 (1989).
[12] S. B. Dierker and P. Wiltzius, Phys. Rev. Lett. **66**, 1185 (1991).
[13] N. J. Wilkinson, M. A. Alam, J. M. Clayton, R. Evans, H. M. Fretwell, and S. G. Usmar, Phys. Rev. Lett. **69**, 3535 (1992).
[14] F. Aliev, W. I. Goldburg, and X.-l. Wu, Phys. Rev. E **47**, R3834 (1993).
[15] M. Y. Lin, S. K. Sinha, J. M. Drake, X.-l. Wu, P. Thiyagarajan, and H. B. Stanley, Phys. Rev. Lett. **72**, 2207 (1994).
[16] S. Lacelle, L. Tremblay, Y. Bussière, F. Cau, and C. G. Fry, Phys. Rev. Lett. **74**, 5228 (1995).
[17] M. Chan, N. Mulders, and J. Reppy, Phys. Today **49** (8), 30 (1996).
[18] D. J. Tulimieri, J. Yoon, and M. H. W. Chan, Phys. Rev. Lett. **82**, 121 (1999).
[19] F. Brochard and P. G. de Gennes, J. Phys. (France) Lett. **44**, 785 (1983); P. G. de Gennes, J. Phys. Chem. **88**, 6469 (1984).
[20] L. Monette, A. J. Liu, and G. S. Grest, Phys. Rev. A **46**, 7664 (1992).
[21] A. J. Liu, D. J. Durian, E. Herbolzheimer, and S. A. Safran, Phys. Rev. Lett. **65**, 1897 (1990).
[22] A. J. Liu and G. S. Grest, Phys. Rev. A **44**, R7894 (1991).
[23] J. P. Donley and A. J. Liu, Phys. Rev. E **55**, 539 (1997).
[24] W. G. Madden and E. D. Glandt, J. Stat. Phys. **51**, 537 (1988); W. G. Madden, J. Chem. Phys. **96**, 5422 (1992).
[25] J. A. Given, Phys. Rev. A **45**, 816 (1992); J. A. Given and G. Stell, J. Chem. Phys. **97**, 4573 (1992).

[26] M. L. Rosinberg, G. Tarjus, and G. Stell, J. Chem. Phys. **100**, 5172 (1994).
[27] D. M. Ford and E. D. Glandt, J. Chem. Phys. **100**, 2391 (1994).
[28] D. M. Ford and E. D. Glandt, Phys. Rev. E **50**, 1280 (1994).
[29] E. Pitard, M. L. Rosinberg, G. Stell, and G. Tarjus, Phys. Rev. Lett. **74**, 4361 (1995).
[30] J. P. Hansen and I. R. McDonald, *Theory of Simple Liquids* (Academic, New York, 1976).
[31] E. Lomba, J. A. Given, G. Stell, J. J. Weis, and D. Levesque, Phys. Rev. E **48**, 233 (1993).
[32] A. Meroni, D. Levesque, and J. J. Weis, J. Chem. Phys. **105**, 1101 (1996).
[33] K. S. Page and P. A. Monson, Phys. Rev. E **54**, R29 (1996); **54**, 6557 (1996).
[34] A. Trokhymchuk and S. Sokolowski, J. Chem. Phys. **109**, 5044 (1998).
[35] P. A. Gordon and E. D. Glandt, J. Chem. Phys. **105**, 4257 (1997).
[36] M. P. Allen and D. J. Tildesley, *Computer Simulations of Liquids* (Clarendon, Oxford, 1987).
[37] E. Kierlik, M. L. Rosinberg, G. Tarjus, and P. A. Monson, J. Chem. Phys. **106**, 264 (1997); **110**, 689 (1999).
[38] A. M. Ferrenberg and R. W. Swendsen, Phys. Rev. Lett. **61**, 2635 (1988).
[39] B. A. Berg and T. Neuhaus, Phys. Rev. Lett. **68**, 9 (1992).
[40] N. B. Wilding, Phys. Rev. E **52**, 602 (1995).
[41] H.-P. Deutsch, J. Stat. Phys. **67**, 1039 (1992).
[42] A. Z. Panagiotopoulos, Mol. Phys. **61**, 813 (1987).
[43] K. K. Mon and K. Binder, J. Chem. Phys. **96**, 6989 (1992).
[44] A. D. Bruce, Phys. Rev. E **55**, 2315 (1997).
[45] A. M. Ferrenberg and D. P. Landau, Phys. Rev. B **44**, 5081 (1991).
[46] R. Evans, J. Phys.: Condens. Matter **2**, 8989 (1990).